CHAPTER THREE
GEOMETRIC MODELLING

3.1 INTRODUCTION

In a traditional macro-cell type wireless communication scheme, the base station would be on some elevated tower and not be surrounded by many close local scatterers, while the receiver would most probably be at ground level, either in a building, automobile or on the street, which would be surrounded by many local scatterers. Investigations in [37, 64, 82] focused on the spatial correlation effects for the above scenario, where the scattering could vary from isotropic to highly non-isotropic scattering.

With the opportunity for wireless local area networks achieving very high data rates for multiple users, the space-time correlation of such channels needs to be investigated [82] so that adequate and appropriate channel models can be adopted. The geometrically based modelling approach used in [64, 83, 84] is considered, but applied specifically for an indoor fixed wireless environment [85] with different scattering PDF configurations at the transmitter and receiver, with the derivation of space-time correlation function. For the fixed wireless scenario considered herein, isotropic scattering at the transmitter end is considered, while the angular distribution of the scatterers at the receiver follows the von Mises probability distribution function (PDF) [64]. The approach used here is to derive the joint space-time correlation function and then separate the transmit antenna and receive antenna correlation. Consequently one derives expressions for the transmit antenna correlation in terms of antenna element spacing and the receive antenna correlation in terms of the scattering parameter k, antenna element spacing $d_{pn},\ d_{mn}$ and mean direction of angle of arrival (AOA), ϕ_R. The

closed form solutions herein presented enables one to determine the effect on the capacity in such a system based on the effects of scattering, antenna element spacing, angular orientation of antenna array and number of antenna elements employed.

3.2 MODEL DESCRIPTION

The new geometric MIMO channel model was initially described after which the mathematical analysis was developed. The new antenna cross correlation function is derived from the mathematical analysis and is based on the below mentioned assumptions.

The new geometric model for a two element transmit antenna and a two element receive antenna (referred here-in as a 2 x 2 MIMO channel, shown in Figure 3.1) is developed by using the multi-element antenna system in [64] as a basis. The fixed receiver/user has a multi-element antenna system with receiver elements RE_m, $RE_n, ...RE_x$; where $x = 2$ here. In this case the 2 x 2 MIMO channel antenna elements form a uniform linear array (ULA) of monopoles that radiate omni-directionally. From the scatterers at TS_l, from the transmitter there is a very narrow dominant beamwidth and the receiver obtains the signal from a large number of surrounding local scatterers, that need not necessarily be isotropic, but the scatterers impinge at point RS_i, as shown in Figure 3.1. It is also assumed that the i^{th} scatterer is planar and could be the sum of different coherent scatterers, which can be of distance R from the center O_R of the RX antenna array.

D is the distance between the transmitter and the receiver and the angles α_{pq} and β_{mn} are the angles the antenna arrays form with the horizontal axis at the transmitter and receiver, respectively. The planar wave formed by the scattering around the receiver can be represented as the angle from the point ϕ_R to the point RS_i. Similarly there are l omnidirectional scatterers at the TX and they lie on a ring of radius L. The l^{th} scatterer at the TX is denoted by TS_l, and θ_T is the angle from the horizontal axis of the antenna array and this scatterer. It is assumed that in this indoor environment the local scattering at the TX is omni-directional and the radius of scatters is very small, that is $L \ll D$ and $L < R$. It is also assumed that the angle of the arc that O_T would form on the circumference of circle O_R is small (typically less than 15^0) [86], for $D \gg R$, that is the angle formed between TS_l and RS_i is small. In this model the line of sight (LOS) component is not considered, but a Rayleigh PDF in a picocell type environment is

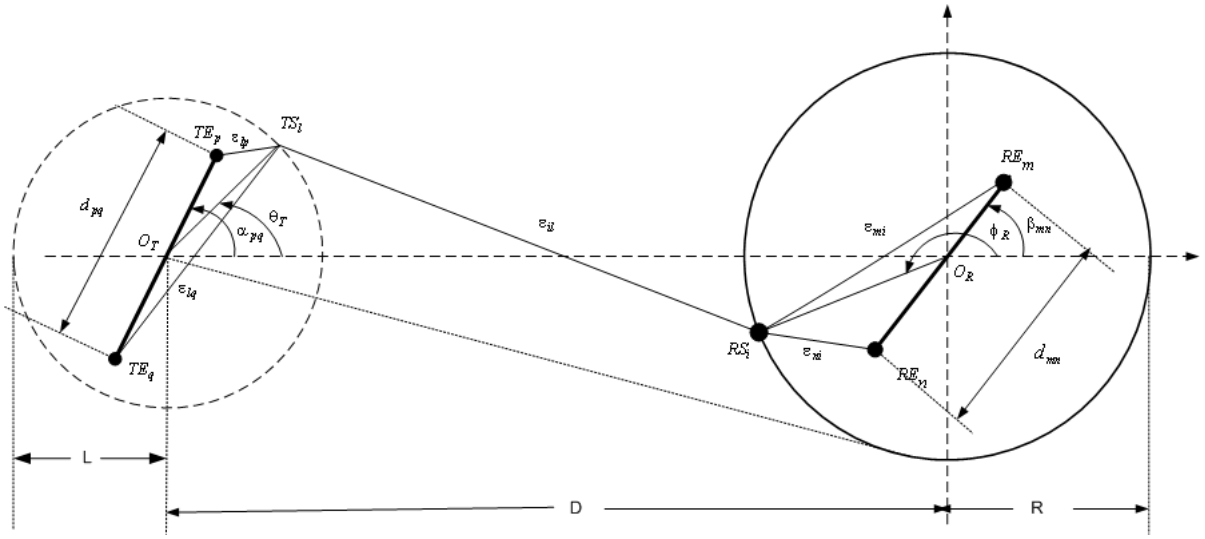

FIGURE 3.1: Geometric Model for a 2x2 MIMO channel

assumed. This MIMO system can be written using the complex baseband notation as

$$\mathbf{y}(t) = \mathbf{H}(t) * \mathbf{x}(t) + \mathbf{n}(t) \tag{3.1}$$

where $\mathbf{H}(t)$ is the channel matrix of complex path gains $h_{ij}(t)$ between TX_j and RX_i, $\mathbf{n}(t)$ is the complete envelope of the AWGN with zero mean from each receive element, $\mathbf{x}(t)$ is the transmit vector made up of the signal transmitted from each TX, $n_t \times 1$ antenna element and $\mathbf{y}(t)$ is the receive vector made up of the signal from each point RS_i.

It is assumed that any gain and phase shift introduced by a scatterer at the transmitter is different to that received at point RS_i. Also, the scatterers at point RS_i are of approximately the same angle, implying that the gain and phase shift is the same at point RS_i and the scatterers do not change with time (that is fixed) in this case. It is also assumed that

$$\lim_{L,N\to\infty} \frac{1}{L}\frac{1}{N} \sum_{i=1}^{L}\sum_{i=1}^{N} E[g_{il}^2] = 1 \tag{3.2}$$

where g_{il} is the amplitude of the wave that comprises of the joint gain of scatterers TS_l and RS_i and L, N are the number of independent scatterers TS_l around the TX, and RS_i around the RX, respectively.

Based on the statistical properties of the described channel, the central limit theorem implies that h_{mp} is a low pass, zero mean, complex Gaussian random process. This means that the envelope $|h_{mp}(t)|$ is a Rayleigh (fading) process. Hence, for the above no line of sight (NLOS),

frequency non-selective, MIMO fading channel propagation scenario, the channel gain, $h_{mp}(t)$, for the link $TE_p - RE_m$ as shown in Figure 3.1, can be written as

$$h_{mp}(t) = \sqrt{\Omega_{mp}} \lim_{L,N\to\infty} \frac{1}{\sqrt{LN}} \sum_{l=1}^{L} \sum_{i=1}^{N} g_{il} \times \exp\left\{ j\psi_{il} - \frac{j2\pi}{\lambda} \left[\varepsilon_{lp} + \varepsilon_{il} + \varepsilon_{mi}\right] \right\} \tag{3.3}$$

where $\psi_i l$ is the joint phase shift introduced by the l_{th} scatterer at TS_l and the i^{th} scatterer at RS_i, $\{\psi_{il}\}_{i,l=1}^{\infty}$ is the iid random process with uniform distribution over the interval $[-\pi, \pi]$, ϵ_{lp}, ϵ_{il} and ϵ_{mi} are the distances as shown in Figure 3.1 which are functions of the angle of departure (AOD) and angle of arrival (AOA), Ω_{mp} is the power transferred through the link from transmit antenna p, through to receive antenna m and λ is the wavelength of the carrier RF signal.

The transpose of the channel gain, $h_{nq}(t)$, for the link $TE_q - RE_n$ shown in Figure 3.1 is

$$h^*_{nq}(t) = \sqrt{\Omega_{nq}} \lim_{L,N\to\infty} \frac{1}{\sqrt{LN}} \sum_{l=1}^{L} \sum_{i=1}^{N} g_{il} \times \exp\left\{ -j\psi_{il} + \frac{j2\pi}{\lambda} \left[\varepsilon_{lq} + \varepsilon_{il} + \varepsilon_{ni}\right] \right\} \tag{3.4}$$

where Ω_{np} is the power transferred through the link from TX antenna q, through to RX antenna n.

3.3 MODEL ANALYSIS

Using the geometric model described in the previous section as a basis, a joint space-time cross correlation function is derived.

The space-time correlation between the two links, $TE_p - RE_m$ and $TE_q - RE_n$, as shown in Figure 3.1, can be defined as

$$\rho_{mp,nq}(\tau) = E[h_{mp}(t).h^*_{nq}(t+\tau)/\sqrt{\Omega_{mp}\Omega_{nq}}] \tag{3.5}$$

where τ is an arbitrary time delay, $*$ indicates the complex conjugate and $\Omega_{mp,nq}$ is the power transfer through $TE - RE$ in a specific $TE_{p,q} - RE_{m,n}$ antenna link element.

The cross correlation function for the scenario in Figure 3.1 can be represented independently of D accordingly as

$$\rho_{mp,nq}(\tau) = \lim_{L,N\to\infty} \frac{1}{L}\frac{1}{N} \sum_{l=1}^{L} \sum_{i=1}^{N} E[g_{il}^2] \times \exp\left\{ \frac{-j2\pi}{\lambda} \left[\varepsilon_{lp} - \varepsilon_{lq} + \varepsilon_{mi} - \varepsilon_{ni}\right] \right\} \tag{3.6}$$

For large number of scatterers L and N and considering the fact the channel is in a quasi-static state, with the receiver at a fixed position, one can write

$$\rho_{mp,nq}(\tau, t) = \rho_{mp,nq}(\tau) = \rho_{mp,nq} \tag{3.7}$$

and hence re-write (3.6) as an integral form of

$$\rho_{mp,nq} = \int_{-\pi}^{\pi} \int_{-\pi}^{\pi} \exp\left\{ \frac{-2\pi j}{\lambda} \left[\varepsilon_{lp} - \varepsilon_{lq} + \varepsilon_{mi} - \varepsilon_{ni} \right] \right\} \times p(\theta_T) p(\phi_R) d\theta_T d\phi_R \tag{3.8}$$

where $p(\theta_T)$ is the probability distribution function of the uniform scatterers at the TX and $p(\theta_R)$ is the probability distribution function of the scatterers at the RX respectively.

Equation (3.8) can now be written in terms of the scatterer angles shown in Figure 3.1 as

$$\rho_{mp,nq} = \int_{-\pi}^{\pi} \int_{-\pi}^{\pi} \exp\left\{ \frac{-2\pi j}{\lambda} \left[\varepsilon_{\theta p} - \varepsilon_{\theta q} + \varepsilon_{m\phi} - \varepsilon_{n\phi} \right] \right\} \times p(\theta_T) p(\phi_R) d\theta_T d\phi_R \tag{3.9}$$

where $\varepsilon_{\theta p,q}$ is the distance from $TE_{p,q}$ to the ring of scatterers TS_l at an angle θ_T from the scattering center, O_T, and $\varepsilon_{\phi m,n}$ is the distance from $RE_{m,n}$ to the ring of scatterers RS_i at an angle ϕ_R from the scattering center O_R.

Using Figure 3.1 one can write the distances in (3.9) for the TX and RX side using the Cosine Law as

$$\varepsilon_{lp}^2 = L^2 + \frac{d_{pq}^2}{4} - d_{pq} L \cos(\alpha_{pq} - \theta_T) \tag{3.10}$$

$$\varepsilon_{\theta p}^2 = L^2 + \frac{d_{pq}^2}{4} - d_{pq} L \cos(\alpha_{pq} - \theta_T) \tag{3.11}$$

$$\varepsilon_{lq}^2 = L^2 + \frac{d_{pq}^2}{4} + d_{pq} L \cos(\alpha_{pq} - \theta_T) \tag{3.12}$$

$$\varepsilon_{\theta q}^2 = L^2 + \frac{d_{pq}^2}{4} + d_{pq} L \cos(\alpha_{pq} - \theta_T) \tag{3.13}$$

$$\varepsilon_{mi}^2 = R^2 + \frac{d_{mn}^2}{4} - d_{mn} R \cos(\phi - \beta_{mn}) \tag{3.14}$$

$$\varepsilon_{m\phi}^2 = R^2 + \frac{d_{mn}^2}{4} - d_{mn}R\cos(\phi - \beta_{mn}) \tag{3.15}$$

$$\varepsilon_{ni}^2 = R^2 + \frac{d_{mn}^2}{4} + d_{mn}R\cos(\phi - \beta_{mn}) \tag{3.16}$$

$$\varepsilon_{n\phi}^2 = R^2 + \frac{d_{mn}^2}{4} + d_{mn}R\cos(\phi + \beta_{mn}) \tag{3.17}$$

Assuming that $R > L$, $L \gg d_{pq}, d_{mn}$ and $R \gg d_{pq}, d_{mn}$, such that $\frac{d_{pq}^2}{4}$ is negligible with respect to the other terms, one can re-write equations (3.11), (3.13), (3.15), (3.17) as

$$\frac{\varepsilon_{\theta p}^2}{L^2} = 1 - \frac{d_{pq}\cos(\alpha_{pq} - \theta_T)}{L} \tag{3.18}$$

$$\frac{\varepsilon_{\theta q}^2}{L^2} = 1 + \frac{d_{pq}\cos(\alpha_{pq} - \theta_T)}{L} \tag{3.19}$$

$$\frac{\varepsilon_{m\phi}^2}{R^2} = 1 - \frac{d_{mn}\cos(\phi - \beta_{mn})}{R} \tag{3.20}$$

$$\frac{\varepsilon_{n\phi}^2}{R^2} = 1 + \frac{d_{mn}\cos(\phi + \beta_{mn})}{R} \tag{3.21}$$

Now using the relation $\sqrt{1+x} \approx 1 + \frac{x}{2}$ for $|x| \ll 1$, the above equations (3.18) $-$ (3.21) can be simplified to

$$\varepsilon_{\theta p} \approx L - \frac{d_{pq}}{2}\cos(\alpha_{pq} - \theta) \tag{3.22}$$

$$\varepsilon_{\theta q} \approx L + \frac{d_{pq}}{2}\cos(\alpha_{pq} - \theta) \tag{3.23}$$

$$\varepsilon_{m\phi} \approx R - \frac{d_{mn}}{2}\cos(\phi - \beta_{mn}) \tag{3.24}$$

$$\varepsilon_{n\phi} \approx R + \frac{d_{mn}}{2}\cos(\phi - \beta_{mn}) \tag{3.25}$$

One can write the joint correlation in (3.7) as an approximate product of transmit antenna and receiver antenna correlation [1, 64, 71].

$$\rho_{mp,nq} = \rho_{pq}^{TX} \rho_{mn}^{RX} \tag{3.26}$$

Hence

$$\rho_{pq}^{TX} = \int_{-\pi}^{\pi} \exp\left\{\frac{-j2\pi}{\lambda}\left[\varepsilon_{\theta p} - \varepsilon_{\theta q}\right]\right\} p(\theta_T) d\theta_T \tag{3.27}$$

and

$$\rho_{mn}^{RX} = \int_{-\pi}^{\pi} \exp\left\{\frac{-j2\pi}{\lambda}\left[\varepsilon_{m\phi} - \varepsilon_{n\phi}\right]\right\} p(\phi_R) d\phi_R \tag{3.28}$$

It is assumed that this TX could be for example in a wide-open hallway, where there is uniform (isotropic) scattering around the close proximity of L for this uniform linear array. This will herein be represented by a PDF [37], $p(\theta_T) = \frac{1}{2\pi}$. Substituting (3.22) and (3.23) and for $p(\theta_T)$ into (3.27), one can re-write (3.27) as

$$\rho_{pq}^{TX} = \int_{-\pi}^{\pi} \exp\left\{\frac{-j2\pi}{\lambda}\left[-d_{pq}\cos(\alpha_{pq} - \theta_T)\right]\right\} \frac{1}{2\pi} d\theta_T \tag{3.29}$$

By applying the trigonometric functions in [87], one can reduce (3.29) to

$$\rho_{pq}^{TX} = \frac{1}{2\pi} \int_{-\pi}^{\pi} \exp jc_{pq}\left[\sin\alpha_{pq}\sin\theta_T + \cos\alpha_{pq}\cos\theta_T\right] d\theta_T \tag{3.30}$$

where $c_{pq} = \frac{2\pi d_{pq}}{\lambda}$

Assuming that the scattering distribution at the RX side follows the von Mises PDF [64] given as:

$$p(\phi) = \frac{\exp\left[k\cos(\phi - \mu)\right]}{2\pi I_0(k)} \tag{3.31}$$

where $I_0(\cdot)$ is the zero-order modified Bessel function, $\phi \in [-\pi, \pi)$, $\mu \in [-\pi, \pi)$ is the mean direction of the AOA seen by the user, and k is the isotropic scattering parameter.

Substituting (3.31) into (3.28), one can re-write (3.28) as

$$\rho_{mn}^{RX} = \frac{1}{2\pi I_o(k)} \int_{-\pi}^{\pi} \exp\left\{\frac{j2\pi d_{mn}}{\lambda}\cos(\phi_R - \beta_{mn}\right\} \exp\left\{k\cos(\phi_R - \mu)d\phi_R\right\} \tag{3.32}$$

Setting $b_{mn} = \frac{2\pi d_{mn}}{\lambda}$, (3.32) can be written as

$$\rho_{mn}^{RX} = \frac{1}{2\pi I_o(k)} \int_{-\pi}^{\pi} \exp\left\{jb_{mn}\cos(\phi_R - \beta_{mn}) + k\cos(\phi_R - \mu)\right\} d\phi_R \tag{3.33}$$

Using the trigonometric functions in [87], (3.33) can be reduced to

$$\rho_{mn}^{RX} = \frac{1}{2\pi I_o(k)} \int_{-\pi}^{\pi} \exp\left\{\sin\phi_R\left[jb_{mn}\sin\beta_{mn} + \sin\mu\right]\right\} \times \exp\left\{\cos\phi_R\left[jb_{mn}\cos\beta_{mn} + k\cos\mu\right]\right\} d\phi_R \tag{3.34}$$

Using the integration rule in [87], equation $3.338 - 4$, page 336 is given as

$$\int_{-\pi}^{\pi} \exp(y\sin x + z\cos x).dx = 2\pi I_0(\gamma) \tag{3.35}$$

where $\gamma = \sqrt{y^2 + z^2}$.

Hence one can express (3.30) as

$$\rho_{pq}^{TX} = I_0(jc_{pq}) \tag{3.36}$$

Similarly (3.35) can be applied to (3.34) to give

$$\rho_{mn}^{RX} = \frac{1}{2\pi I_0(k)} \int_{-\pi}^{\pi} \exp\left\{(jb_{mn}\cos(\phi_R - \beta_{mn})) + k\cos(\phi_R - \mu)\right\} d\phi_R \tag{3.37}$$

which is reduced to

$$\rho_{mn}^{RX} = \frac{1}{I_0(k)} I_0((jb_{mn}\sin\beta_{mn} + k\sin\mu)^2 + (jb_{mn}\cos\beta_{mn} + k\cos\mu)^2)^{1/2} \tag{3.38}$$

Applying the basic trigonometric identities to (3.38) and simplifying it gives

$$\rho_{mn}^{RX} = \frac{1}{I_0(k)} I_0\left(k^2 - b_{mn}^2 + j2kb_{mn}\cos(\mu - \beta_{mn})\right)^{1/2} \tag{3.39}$$

where $b_{mn} = \frac{2\pi d_{mn}}{\lambda}$.

The closed form expressions for the antenna correlations are represented in equations (3.36) and (3.39) for the TX and RX respectively. This allows one to solve these expressions analytically in order to determine some of the model characteristics and its impact on the capacity of the MIMO system.

3.4 RESULTS

The spatially and temporally correlated variates are generated by generating an $n_R \times n_T$ matrix $\mathbf{U}$, of random, independent and zero mean complex Gaussian variates with unit variance. Using $\mathbf{X} = \mathbf{U}\sqrt{\mathbf{R}_T}$, the $n_R \times n_T$ with the desired transmit antenna correlation is calculated. $\mathbf{R}_T$ is the $n_T \times n_T$ matrix of the transmit antenna correlation, with matrix elements ρ_{pq}^{TX} calculated from (3.39). Matrix $\mathbf{H}$ is then calculated using $\mathbf{X}$ as the input vector with the desired correlation matrix elements calculated from (3.39).

The normalized MIMO channel capacity, C, in b/s/Hz for a particular realization $\mathbf{H}$ can be expressed [9, 15] as

$$C = \log_2 \det\left(I_{n_R} + \frac{\rho}{n_T}\mathbf{H}\mathbf{H}^H\right) \tag{3.40}$$

where $\mathbf{H}^H$ is the conjugate transpose, det is the determinant of the matrix, I_{n_R} is a $n_R \times n_T$ identity matrix, and, ρ is the average SISO SNR at each of the n_R elements.

Many different random channel realizations were considered and the capacity for each of these realizations were computed and then statistically distributed. From this, the cumulative distribution function (cdf) for the capacity was calculated by taking into account the effects of the various parameters derived in the model.

Uniform linear arrays (ULA's) were considered in this case with the following general parameters applied to this model.

SNR = ρ = 20 dB
TX carrier frequency = 2.4 GHz
$\alpha_{pq} = \beta_{mn} = \pi/2$
k = 0.25
D = 20 metres
R = 0.2 metres

Figure 3.2 shows the complimentary cumulative distribution function (ccdf) versus capacity for varying number of TX, n_T, and receiver, n_R, antenna elements. Here $\mu = \pi$, $\lambda = 0.125$,

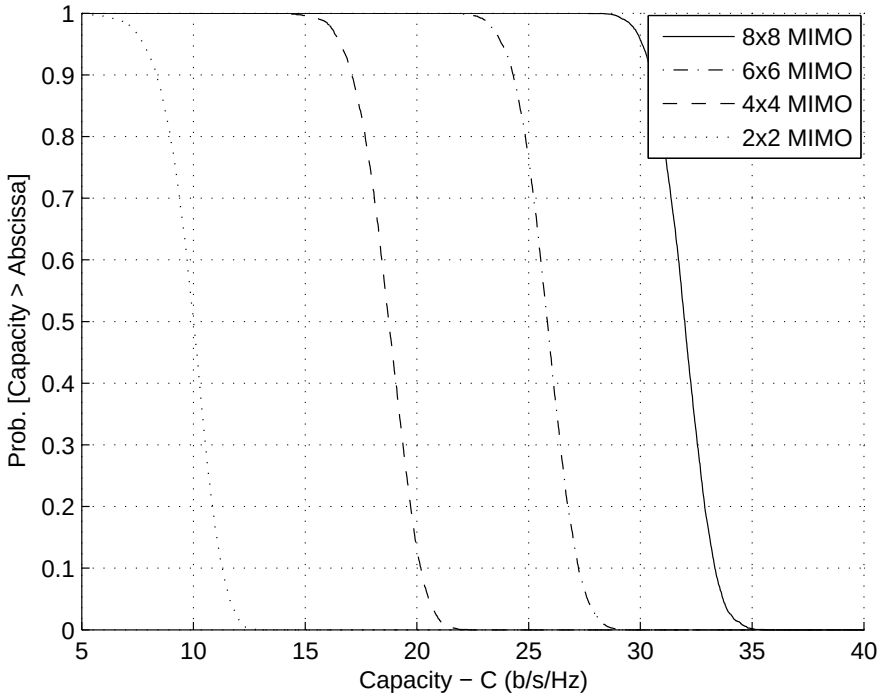

FIGURE 3.2: ccdf versus capacity for varying antenna elements, $n_T = n_R$

$d_{mn} = d_{pq} = 0.5\lambda$, ρ = 20 dB and $k = 25$. One observes [37] that the capacity increases as the number of antenna elements in the MIMO system increases from two to eight elements for some fixed outage probability. Increasing the number of antenna elements, both at the transmitter and receiver ends, makes the greatest impact on the channel capacity when compared to the other parameters. Based on the indoor MIMO measurement campaign undertaken and described herein and in [88], it was observed that for $n_R = n_T = 8$, with SNR = 20 dB, the capacity was 95% accurate for an outage probability greater than 90% for location 2 [89], having characteristics almost identical to the described model.

Figure 3.3 indicates the ccdf for the case where the antenna element spacing d_{mn} is varied from 0.25λ up to 4λ, referred to as d in Figure 3.3. The SNR=20 dB, $k = 25$, $\mu = \pi$, $d_{pq} = 0.5\lambda$ and $n_R = n_T = 2$ were used in the computation.

For the above chosen parameters, one observes that for an outage probability of greater than 95%, the capacity can vary by approximately 2b/s/Hz for $0.25\lambda \leqslant d \leqslant 4.0\lambda$. The RX antenna array element spacing of $d_{mn} > 4.0\lambda$ and for $d_{mn} < 0.25\lambda$ resulted in a negligible effect on

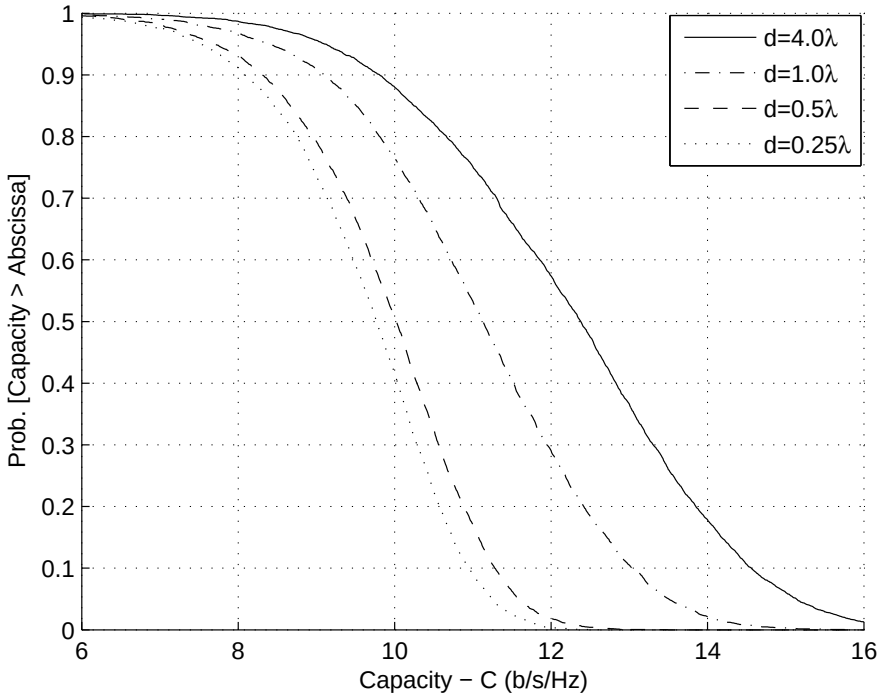

FIGURE 3.3: ccdf versus capacity for varying antenna spacing, d=d_{mn}

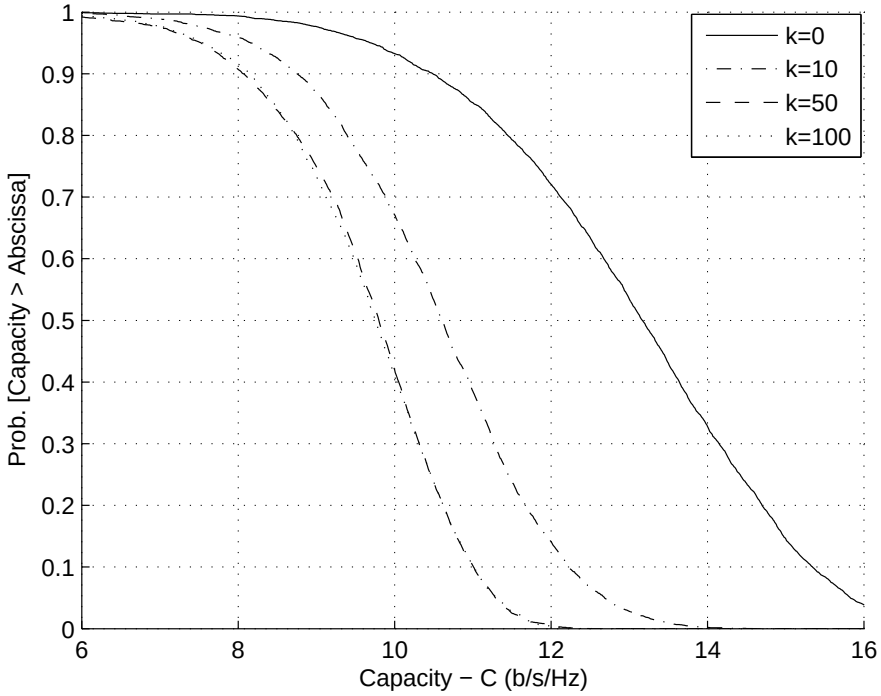

FIGURE 3.4: ccdf versus capacity for varying scattering parameter, k

the capacity for a specific outage probability. As expected, increasing the element spacing d_{pq} resulted in a trend similar to that in Figure 3.3, except that it occurred at a higher capacity.

Figure 3.4 shows the effect of the scattering parameter k on the capacity of the 2×2 MIMO system where the SNR=20 dB and $d_{mn} = d_{pq} = 0.5\lambda$. From the isotropic scattering $(k = 0)$ case to the highly non-isotropic scattering at the RX, the capacity could decrease by less than 2.5 b/s/Hz for an outage probability beyond 95%. One observes that for $k > 50$ the capacity does not vary significantly for some fixed high outage probability. This implies that in an indoor environment where there are significantly large number of local scatterers, using a k value of greater than 50 should not have any significant impact upon the degradation in channel capacity.

For $k = 25$, $n_R = n_T = 2$, $d_{mn} = d_{pq} = \lambda$ and $\rho = 20$ dB the plot of capacity outage probability for the variation in RX antenna array orientation, β_{mn} was determined as shown in Figure 3.5. For the antenna orientation variation from $\pi/2$ to 0 radians, the capacity could decrease by less than 3.0 b/s/Hz for an outage probability of greater than 95%. As expected from a uniform linear antenna array, rotating the RX antenna array between π and $\pi/2$ radians has a similar effect to that as shown in Figure 3.5.

Figure 3.6 validates the developed model behavioral characteristics and confirms the effect of SNR on the channel capacity as proposed in [9]. This was simulated for the parametric settings of $d_{mn} = d_{pq} = 0.5\lambda$, $n_R = n_T = 2$ and $k = 25$. One also observes, as expected, that for an increase of SNR by 3dB the capacity maximally increased by approximately 1 b/s/Hz for an outage probability beyond 90%.

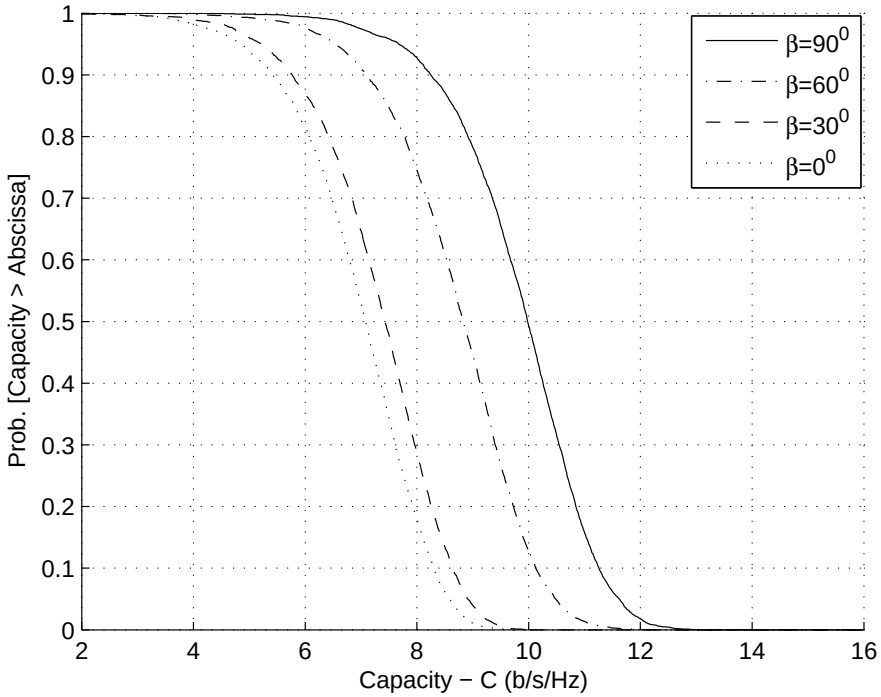

FIGURE 3.5: ccdf versus capacity for varying RX antenna orientation, β

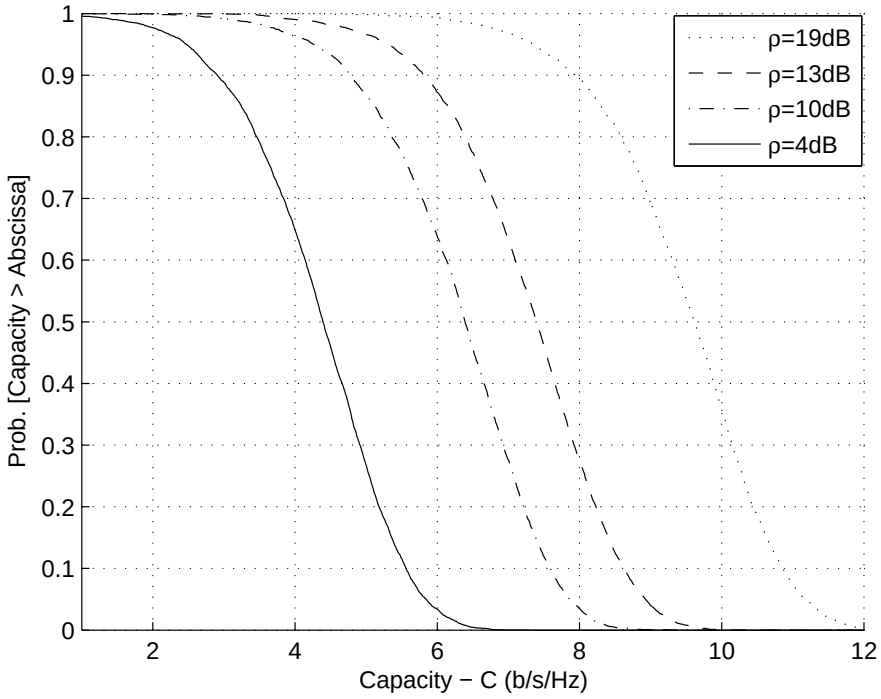

FIGURE 3.6: ccdf versus capacity for varying SNR(ρ) in dB

3.5 CONCLUSION

Performance gains of MIMO systems have been explored by theoretical studies involving stochastic channel models, ray tracing techniques and direct channel measurements. Arguably geometric modelling could be the most cost effective and time efficient technique. A geometrically based model as a way to characterize a MIMO channel in a fixed wireless indoor environment has successfully been derived. The geometric model that was presented led to the derivation of the joint correlation function as well as the receiver and transmitter antenna correlation functions in a neat, compact and closed form. The model incorporates key characteristics such as the type of antennas, configuration of the antenna array, the number of antenna elements, antenna element spacing, degree of scattering at the receive antenna and antenna orientation so as to exploit the MIMO channel performance gains. In comparison to all the described parameters, the increase in the number of antenna elements made the greatest impact and contribution to the increase in channel capacity while antenna spacing affecting the spatial correlation was another significant contributor.